JOURNAL OF SOLID STATE CHEMISTRY 38, 321–334 (1981)

Alkali-Metal-Intercalated Transition Metal Disulfides: A Thermodynamic Model

A. S. NAGELBERG* AND W. L. WORRELL

Department of Materials Science and Engineering, University of Pennsylvania, Philadelphia, Pennsylvania 19104

Received May 19, 1980; in revised form December 22, 1980

In the lithium-intercalated disulfides, Li_xMS_2, where M = Ti,Ta, a nearly linear compositional variation of the lithium chemical potential is observed throughout the composition range $0 < x < 1.0$. For most sodium-intercalated disulfides, chemical potential plateaus are observed between regions exhibiting linear variations of sodium chemical potential. Our thermodynamic model indicates that the two most important factors which determine the compositional variation of the alkali metal chemical potential are the interaction energy between intercalated alkali-metal atoms and the compositional variation of the electron chemical potential. Although these two factors determine the compositional variation of chemical potential in single-phase regions, the existence of two-phase regions in the concentration range $x = 0$–0.15 are influenced by the energy required to expand the interlayer gap and the configurational entropy.

Introduction

In recent years there have been numerous investigations (*1–5*) of nonstoichiometric compounds which can readily and reversibly incorporate an element into their lattice without significantly changing the local atomic coordination or crystal structure. One group of compounds that can easily incorporate alkali-metal atoms into its lattice is the Group IV, V, and VI transition metal dichalcogenides. The dichalcogenides have a layered structure (*1, 6*) in which a hexagonal layer of transition metal atoms (M) is sandwiched between two hexagonal layers of chalcogen (X) atoms. The transition metal atoms in the hexagonal crystal can have either an octahedral or trigonal prismatic coordination of chalcogen atoms. The same chalcogen atom coordinations are possible for the interstitial positions in the weakly bonded gap between X–M–X sandwiches. Intercalation, the incorporation of a metal atom into the interstitial positions within the gap, results in a large expansion perpendicular to the layers. The ionic nature of the intercalated atoms is indicated by the small Knight shifts observed in NMR measurements (*7–10*), e.g., a 3–12 ppm shift for lithium in Li_xTiS_2 compared to 240 ppm in pure lithium.

The compositional variations of the alkali-metal chemical potential of several alkali-metal-intercalated disulfides have been measured electrochemically (*3, 11–16*). The chemical potentials are very negative (<-96 kJ/mole) and are usually a linear function of composition. The magnitude

* Presently at Sandia National Laboratories, Livermore, Calif. 94550.

0022-4596/81/090321-14$02.00/0

and compositional variation of the alkali-metal chemical potentials are important parameters in the analysis of intercalated dichalcogenides as battery cathodes. To function as useful cathode materials, the intercalated alkali-metal atoms must exhibit large negative chemical potentials over extended composition ranges.

McKinnon and Haering (*17*) have recently calculated the strain-induced interaction energies of lithium intercalated phases and have used these values to explain ordering and phase relationships. Armand (*18*) has also derived a model, which considered the entropy of intercalated atoms and the lattice expansion energy, to explain the thermodynamic behavior of intercalated phases. Thompson (*19*) has used lattice gas models to explain the existence of lithium ordering in Li_xTiS_2 measured by a technique developed by Thompson, "Electrochemical Potential Spectroscopy."

The previous models (*17, 18, 31*) do not give an explanation of the large alkali metal chemical potential variations observed for numerous intercalated disulfides. The purpose of this paper is the development of a thermodynamic approach to model the compositional variation of alkali-metal chemical potential in the intercalated disulfides. The model increases our understanding of the behavior of the alkali-metal chemical potential and should be useful in planning future thermodynamic investigations. The influence of four factors on the compositional variation of chemical potential is discussed. The factors considered include the entropy and strain energy of lattice expansion considered previously and two additional significant factors; the interaction energy between intercalated atoms and compositional changes in the electron chemical potential. Our model makes no attempt to calculate the absolute values of the alkali metal chemical potential.

Model

The physical nature of the intercalation process, the occupation of vacant sites in the two-dimensional gap between MX_2 sandwiches, suggests the applicability of a two-dimensional model analogous to the chemisorption of an atom on a surface. In this case the "chemisorption" involves two "surfaces" and adds the restriction that only a "monolayer" occurs. As in the chemisorption phenomena, the activity of the inserted atoms should be influenced by the configurational entropy of the intercalated atoms filling the vacant sites in the gap and the partial molar enthalpy arising from strong bonding to the MX_2 layers. The partial molar enthalpy includes a compositional dependent term arising from the change in electron chemical potential as the electron density increases with increasing concentration of intercalated atoms. As the interlayer sites become filled, another contribution to the partial molar enthalpy is the interactions between inserted atoms, especially when considering intercalated dichalcogenides, where the inserted atoms are highly ionized. Finally, an enthalpy contribution to the chemical potential of the inserted atoms, which does not have an analogous term in the chemisorption phenomenon, involves the energy required to separate and/or shift the dichalcogenide layers sufficiently to accommodate the inserted atoms.

The thermodynamics of absorption for noninteracting atoms was considered by Langmuir (*20*) and Fowler and Guggenheim (*21*). It is found that the chemical potential of the absorbed atoms (A) can be expressed as

$$\mu_A = +RT \ln (\Theta/1 - \Theta) + C, \quad (1)$$

where

Θ is the fraction of available sites filled;

C is a term determined by the interaction of the absorbed atom and substrate.

The concentration dependent term of Eq. (1), $RT \ln (\Theta/1 - \Theta)$, arises from the ways of filling the available surface sites and can be considered analogous to a product of the temperature and configurational entropy.

For our model, we assume that the localized bonding which occurs between the inserted A atom and the MS_2 layers does not vary significantly with composition, thus C is considered concentration independent.

An energy contribution to μ_A arises from the repulsive interactions between the inserted alkali metal atoms. Fowler and Guggenheim (*21*) have considered interactions between nearest neighbor adsorbed atoms and have modified the Langmuir isotherm to yield Eq. (2):

$$\mu_A = RT \ln (\Theta/1 - \Theta) + z\omega\Theta + C \quad (2)$$

for the chemical potential, where ω is the lateral interaction energy within the interlayer gap, and z is the coordination number within the gap. The first term in Eq. (2) is obtained assuming a completely random occupation of sites in the interlayer gap, which becomes less applicable as the interaction energy ω increases.

The interaction energy term $z\omega\Theta/RT$ in Eq. (2) represents only the repulsive interaction between inserted atoms. When an atom is inserted, it donates an electron to the MS_2 layers and the energy contribution to the alkali metal chemical potential will change as the electron density changes. The transition metal dichalcogenides of Groups IV and V are reported to be either narrow-band d metals or narrow-gap semiconductors (*6, 22, 23*). For the compounds that are narrow-band d metals, the half-filled d_{z^2} band is typically 1 eV in width (*22*). Assuming that the alkali metal atom is fully ionized and the band has a total of 2 states per MS_2 molecule and is 1 eV in width, the relationship between the electron chemical potential (μ_F) and composition x can be derived and is given by

$$3 (\Delta\mu_F) - 4 (\Delta\mu_F)^3 = x, \quad (3)$$

where

$$\Delta\mu_F = (\mu_F - \mu_F^0)$$

and

μ_F is the electron chemical potential;

μ_F^0 is the electron chemical potential for the pure dichalcogenide.

Equation (3) assumes that the d_{z^2} electron band has a parabolic density of states function. The variation of the electron chemical potential with x in A_xMS_2 calculated from Eq. (3) is shown in Fig. 1. The slope of the curve is essentially constant for concentrations below $x = 0.8$. At the higher concentrations, $\Delta\mu_F$ changes rapidly until reaching ~0.5 eV, half the d_{z^2} band width. Since the electron energy bands will tend to shift in energy in an attempt to maintain a constant electron chemical potential during a charge transfer process, the values given by Eq. (3) would overestimate the electron chemical potential variation. For the narrow-gap semiconductors, a similar empirical relationship is not easily derived. Nonhomogeneous electron theory (*24*) can also be used to estimate the compositional variation of the electron chemical potential. The theory assumes a Thomas–Fermi electron gas

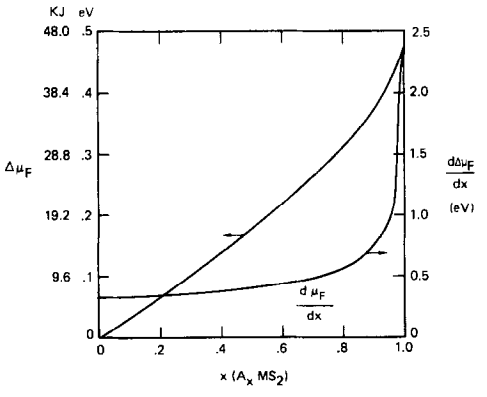

FIG. 1. Calculated compositional variation of electron chemical potential ($\Delta\mu_F$) and electron chemical potential gradient, ($d\mu_F/dx$).

modified by exchange and correlation energy terms. Numerous equations have been developed to express the variation of the electron chemical potential with electron density (*24*), and all exhibit nearly linear variations of the electron chemical potential for the electron densities encountered in the dichalcogenides. The magnitude of the change of μ_F for the transition from an unintercalated to a fully intercalated dichalcogenide is about 0.4 eV which is similar to that shown in Fig. 1. Thus the relationship given by Eq. (3) and Fig. 1 is a reasonable approximation of the compositional variation of the electron chemical potential. The energy contribution to the alkali metal chemical potential, μ_A, is given by $F\, d\mu_F/dx$, where F is Faraday's constant.

The fourth major contribution to the compositional variation of alkali-metal chemical potential arises from the energy required to expand the interlayer gap. Armand (*18*) has calculated the compositional variation and magnitude of the interlayer expansion energy in intercalated graphite assuming that at small concentrations of intercalated species, the lattice expands locally. In Armand's calculations, the partial molar enthalpy of expansion was assumed to be inversely proportional to the fraction of sites filled in the interlayer gap. In our model, the lattice expansion energy was calculated using Armand's approach (*18*) and the measured c-axis expansion of the alkali-metal intercalated disulfides (*3, 11, 25, 26*).

Combination of the measured variation of the c-axis with composition and the variation of the interlayer force as a function of separation permits calculation of the expansion contribution as $B(dc/dx)$, where B is the interlayer force given by the Lennard–Jones potential function as (*18*)

$$B = \left[\frac{1}{6k}\left(\frac{c_0}{c}\right)^5 - \left(\frac{c_0}{c}\right)^{11}\right], \qquad (4)$$

where

k is the compressibility parallel to the c-axis;

c is the c-axis lattice parameter;

and

c_0 is the c-axis lattice parameter for the unintercalated disulfide.

The constants in the Lennard–Jones potential function are obtained from the boundary conditions that the force at equilibrium spacing in the pure disulfide is zero and that the change in force with separation is given by the reciprocal of the compressibility. An increase in compressibility indicates that it is easier to expand or contract the interlayer gap. The reported compressibilities of MoS_2, NbS_2, HfS_2, and $NbSe_2$ are 10–20 $\times$ 10^{-13} cm^2/dyne (*27–30*). Because the crystal stoichiometry was not characterized, some excess transition metal probably exists in the van der Waals gap, and the experimental values of compressibility are probably too low. The compressibility of graphite, a similar layered structure with van der Waals bonding between layers, is 30 $\times$ 10^{-13} cm^2/dyne, which may be a more reasonable value for the disulfides (*31*).

The contribution of the lattice expansion energy to the alkali metal chemical potential is most significant at low compositions where the c-axis expands rapidly. The magnitude of the contribution is typically large enough to predict immiscibility or phase separation at low concentrations. Immiscibility arises because the expansion energy per inserted atom is large at low compositions. At extremely low concentrations this energy term is offset by the entropy contribution. The entropy term increases rapidly and a composition range is reached in which the expansion energy term is no longer offset. In this composition range, our model predicts that the stable phases would be the extremely low concentration phase where the entropy contribution is significant and a higher concentra-

tion phase in which the only significant contributions are the repulsive interaction energy (ω) and compositional variation of the electron chemical potential.

The concentration range in which phase separation would occur is controlled by the energy terms discussed previously. An increase in the force required to separate the layers and a decrease in the pairwise interaction energy and electron chemical potential variation causes an enlarged phase separation range. Even if a nonrigid layer is considered in calculating the lattice expansion energy term, a two-phase region is expected for all but the smallest interlayer forces (B). For sufficiently large interlayer forces (B) and small interaction energies (ω), multiple stage compounds can exist (*3*). In a multiple state compound, atoms are not intercalated into every interlayer gap. For example in a Stage II compound, atoms are intercalated into every other interlayer gap as contrasted to a Stage I compound, where atoms are intercalated into every interlayer gap. The energy required to expand an interlayer gap makes it energetically favorable to intercalate atoms into only a few gaps. Conversely, the contribution of the entropy and interaction energy terms is minimized when inserted atoms occupy many interlayer gaps. The location of any two-phase regions caused by an immiscibility or formation of multistage compounds at lower compositions ($x < 0.3$) is very sensitive to the magnitude of the interlayer force and the method by which the lattice expansion energy is calculated.

When the lattice expansion contribution and electron chemical potential variation are considered, Eq. (2) can be rewritten as

$$\mu_A = RT \ln (\Theta/1 - \Theta) + z\omega\Theta + F(\mu_F(x) - \mu_F^0) + B(dc/dx) + \text{const.} \quad (5)$$

The relationship given by Eq. (5) cannot be applied to the intercalated dichalcogenides until the relationship between the fraction of available sites (Θ) and the composition (x) is known. Two different types of interlayer stacking have been reported (*3*); hexagonal close-packed and hexagonal. In the hexagonal close-packed stacking, trigonal antiprismatic (TAP) sites and tetrahedral sites exist. The occupation of the tetrahedral sites by intercalated atoms is unlikely from size considerations (*3*). For example, in the fully expanded lattice of Na_xTaS_2, the maximum radius of an atom that can fit in the tetrahedral site is 0.8 Å, while the ionic radius of sodium if 0.95 Å. The occupation of a tetrahedral site is thus energetically unfavorable and is assumed to be nil. Neutron diffraction studies of Li_xTiS_2 have shown that lithium occupies only the TAP sites (*3*). Therefore in this hexagonal close-packed stacking, $x = \Theta$, with $z = 6$ because there is one octahedral site per MS_2. In the hexagonal stacking, the alkali metal atoms reside in sites with a trigonal prismatic (TP) coordination of sulfur atoms. There are two TP sites per dichalcogenide atom but neighboring sites cannot be occupied simultaneously because of size considerations and the prohibitive interaction energy that would result. For this case, every occupied site excludes the three nearest neighbor sites from being occupied. The number of sites that can be occupied per dichalcogenide molecule, N_A, is the number of sites per dichalcogenide in the TP coordination, 2, decreased by the number of excluded sites, $3x$, with higher-order terms considering multiple counts and is given by Eq. (6)

$$N_A = 2 - 3x + \frac{3x^2}{N_A} - \frac{x^3}{N_A^2}. \quad (6)$$

The value of Θ is given by x divided by N_A. Calculations using Eq. (6) indicate that x is essentially equal to Θ; indeed the difference between x and Θ is never greater than 0.07. Therefore the relationship given by Eq. (5) will be simply applied with $x = \Theta$.

In summary, the compositional variation of the chemical potential of a species intercalated into the transition metal dichalcogenides depends on four major factors. The contribution of each factor is illustrated schematically in Fig. 2 by showing the change in the chemical-potential–composition curve as each energy term is considered. The chemical potential axis in Fig. 2 only expresses the relative change in chemical potential due to the various factors considered above; the value of the constant in Eq. (5) is not considered. In subsequent figures where experimental determinations of the alkali-metal chemical potential are available, actual values are used. The first contribution is the entropy of filling vacant sites in the interlayer gap. This factor is most significant at the composition extremes, where the logarithm term expressing the entropy tends to $\pm\infty$ as seen in curve (a) of Fig. 2. Secondly, the chemical potential is affected by the variation of the electron chemical potential as electrons are donated to the electron bands of the dichalcogenides. Using either a rigid band approximation (Fig. 1) or nonhomogeneous electron gas theory, the electron chemical potential is found to be a nearly linear function of composition. Curve (b) in Fig. 2 shows the added effect of the compositional variation of μ_F given in Fig. 1 to the configurational entropy. The variation of the electron chemical potential with composition is found in curve (b) to increase the average slope of the chemical potential curve, with the high curvature of the μ_F vs composition curve for $x > 0.8$ being minimal compared to the entropy contribution curvature. The third factor is due to the mutual repulsion of intercalated atoms within the gap. The contribution is proportional to the fraction of sites filled for a random occupation, or when there is a low interaction energy. At higher interaction energies larger slopes are observed as shown by curves (c) and (d) (solid lines) in

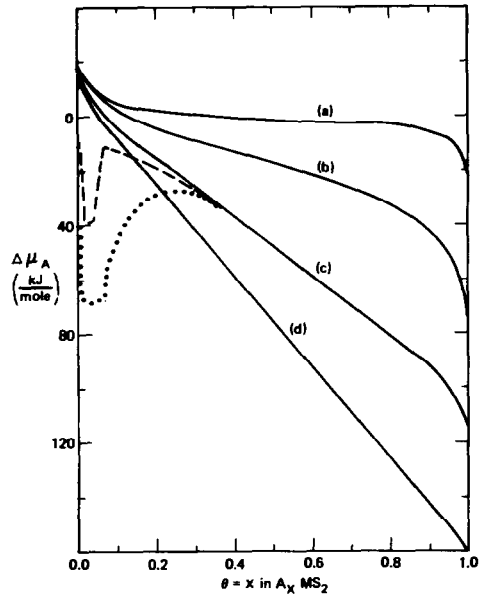

FIG. 2. Predicted compositional variation of alkali metal chemical potential using Eq. (6): (a) $z\omega = 0$, $d\mu_F/dx = 0$; (b) $z\omega = 0$, $d\mu_F/dx$ given in Fig. 1; (c) $z\omega = 50$ kJ/mole, $d\mu_F/dx$ given in Fig. 1; dashed line: $k = 30 \times 10^{-13}$ cm²/dyne; dotted line: $k = 10 \times 10^{-13}$ cm²/dyne; (d) $z\omega = 100$ kJ/mole, $d\mu_F/dx$ is given in Fig. 1.

Fig. 2 for $z\omega = 50$ and 100 kJ/mole, respectively. An increase in the repulsive interaction between intercalated atoms increases the average slope of the chemical potential curve.

Finally at low concentrations, the energy required to separate the dichalcogenide layers can be a significant contribution to the alkali metal chemical potential. The lattice expansion contribution has a very pronounced effect on the chemical potential curve at low compositions where the intercalated disulfide lattice exhibits the largest compositional variation of the c-axis. Including the affect of the interlayer gap expansion energy in the theoretical chemical potential curves is seen in Fig. 2 to cause an increase in chemical potential for values $x < 0.3$. In fact for the broken lines in Fig. 2, a local minima and a maxima are created in the chemical potential curve, identifying a

concentration range of immiscibility. In addition, the lattice expansion energy can play a major role in determining the two-phase compositional ranges between different stage compounds. Although the shape of this contribution of the lattice expansion energy can be calculated if the variation of the c-axis with composition is known, the magnitude can only be estimated by assuming a value for the compressibility of the dichalcogenide. Figure 2 shows the affect of this contribution for compressibilities of 30 $\times$ 10^{-13} cm^2/dyne (dashed line) and 10 $\times$ 10^{-3} cm^2/dyne (dotted line) on curve (c) for $z\omega$ = 50 kJ/mole, using the variation of c-axis for Na_xTaS_2 (*26*) and Eq. (5) for the interlayer force, B.

Application of Model to Sodium-Intercalated Disulfides

Experimentally, the chemical potential can be conveniently measured by electrochemical techniques. The conversion of the chemical potential measured in kilojoules per mole to volts is classically stated by the Nernst equation. For the alkali metals, the value of n is one and the proportionality between the two units is simply Faraday's constant, 96,473 J/mole/volt. In the following discussion, alkali-metal chemical potentials will be stated in kilojoules per mole and figures are plotted with the chemical potential becoming less negative from top to bottom.

At compositions where there is negligible expansion of the c-axis, the slope of the alkali-metal chemical potential curve given by Eq. (5) is essentially determined by the value of alkali–alkali-metal interaction energy (ω) and the variation of electron chemical potential, since the entropy is a very minor contribution. An empirical value of ω is determined by measuring the slope of the line and subtracting the compositional variation of electron chemical potential, $d\mu_F/dx$ to yield $z\omega$. An independent determination of ω and $d\mu_F/dx$ using Eq. (5) is not possible. An error of 19.3 kJ (0.2 eV) in the magnitude of the μ_F variation will result in an error of 3.3 kJ/mole in the value of ω. The locations of possible two-phase regions are determined by considering the effect of the lattice expansion energy. The lattice expansion contribution is determined from Eq. (4) and is independent of the valves for ω and $d\mu_F/dx$.

The compositional variation of the sodium chemical potential in Na_xTaS_2 (*13*) is shown in Fig. 3. Using the variation of μ_F given by Fig. 1, the slope of the chemical potential curve, and Eq. (5), a value of the interaction energy (ω) equal to 20.5 kJ/mole is obtained for z = 6. A small chemical potential plateau is drawn for $x <$ 0.1 and indicates a possible immiscibility

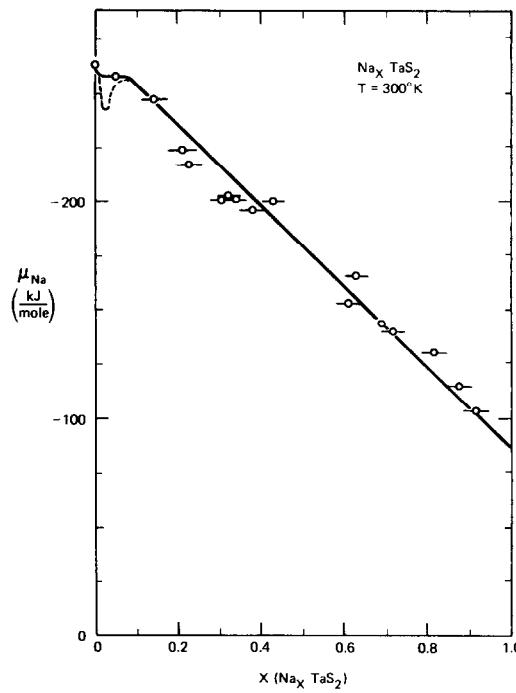

FIG. 3. Compositional variation of sodium chemical potential of Na_xTaS_2 at 300 K (*13*). Solid line is the model curve (Eq. (5) when ω = 20.5 kJ/mole and k = 30 $\times$ 10^{-13} cm^2/dyne). Dotted line represents the metastable chemical potential curve.

when considering the effects of lattice expansion energies. The increase in chemical potential (decrease in voltage) shown by the dashed line in Fig. 3 for $k_c = 30 \times 10^{13}$ cm²/dyne leads to an instability and thus an immiscibility.

Another interpretation of the measured sodium chemical potential of Na_xTaS_2 involves a voltage plateau for $0.3 < x < 0.42$. Previously (*13*) it was concluded that the plateau was only an artifact of the experimental scatter because the measured voltages in this composition region were within the least-squares uncertainty limits of the straight line shown in Fig. 3. Application of the thermodynamic model to this second interpretation yields the curves shown in Fig. 4. The first plateau for $x < 0.05$ reflects the predicted immiscibility in the first compound. The first compound would be stable until $x = 0.30$. For the composition range $0.3 < x < 0.42$, a second phase of the composition $Na_{0.42}TaS_2$ would coexist with the first phase of the composition $Na_{0.3}TaS_2$. For compositions above $x = 0.42$ only the second compound, $Na_{0.42}TaS_2$, would exist. When two phases can exist in the same composition range, equilibrium does not simply occur when one chemical potential curve crosses another in a plot of μ_A vs x. The equilibrium composition is derived in the Appendix and is defined by Eq. (7)

$$\int_{-\infty}^{\mu_a} (x'' - x')d\mu = 0, \qquad (7)$$

where

x' is the composition of phase 1 as a function of chemical potential;

x'' is the composition of phase 2 as a function of chemical potential;

μ_a is the equilibrium chemical potential.

Graphically, Eq. (7) requires the two shaded areas shown in Fig. 5 to be equal. The calculated interaction energies from application of the model to the two-phase interpretation of Na_xTaS_2 are 35.6 and 24.3 kJ/mole for the first and second compounds, respectively. Values of the interaction energies calculated for both the one phase and a two-phase interpretation involving a Stage I and Stage II phase of Na_xTaS_2 are given in Table I. The experi-

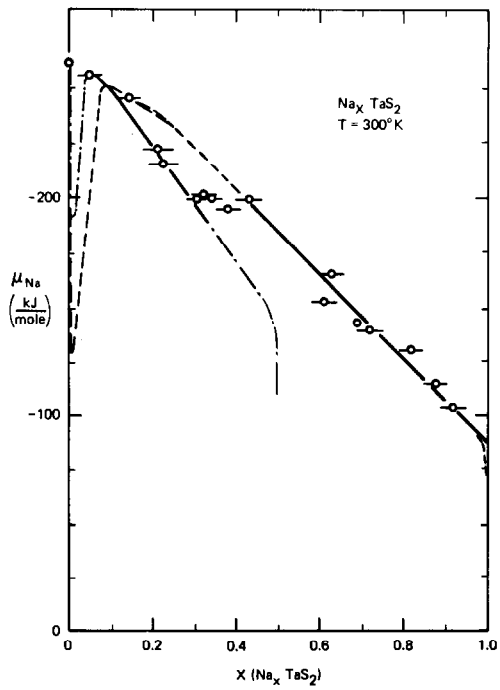

FIG. 4. Thermodynamic model curves for Na_xTaS_2 at 300 K (*13*): (– – –) assuming a Stage I compound; ω = 24.3 kJ/mole and $k = 30 \times 10^{-13}$ cm²/dyne; (–·–) assuming a Stage II compound; ω = 35.6 kJ/mole and $k = 30 \times 10^{-13}$ cm²/dyne.

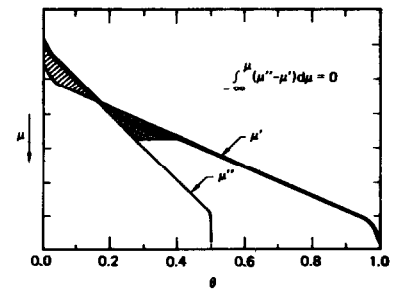

FIG. 5. Graphic determination of two-phase equilibria between intercalated dichalcogenide phases.

TABLE I

CALCULATED ALKALI–ALKALI-METAL INTERACTION ENERGIES (ω) FOR SODIUM- AND LITHIUM-INTERCALATED DISULFIDES

Compound	Composition range (Stage)	Alkali–alkali-metal interaction energy; (ω) (kJ/mole)
Na_xTaS_2[a]	$0.10 < X < 1.0$	20.5[b]
Na_xTaS_2[c]	$0.05 < X < 0.3$ (II)	35.6
	$0.42 < X < 1.0$ (I)	24.3
Na_xTiS_2	$0.10 < X < 0.20$ (II)	10.9
	$0.35 < X < 0.60$ (I)	22.6
	$0.70 < X < 1.0$ (I)	11.7 ± 6
Li_xTaS_2	$0.0 < X < 1.0$ (I)	17.2
Li_xTiS_2	$0.0 < X < 1.0$ (I)	2.9
Li_xVS_2	$0.0 < X < 1.0$ (I)	~0.0

[a] Interpretation with no Stage II compound formation.

[b] Uncertainty is ±4 kJ/mole for all numbers in this column except where indicated.

[c] Interpretation with a Stage II compound formation.

mentally measured sodium chemical potentials in Na_xTaS_2 exhibit too much scatter to differentiate between the two interpretations, and the physical differentiation of two phases has not been observed.

The proposed two phases could be a Stage II compound at low compositions and a Stage I compound at high compositions, as illustrated by the theoretical curves shown in Fig. 4. A second interpretation could be that the two-phase region $0.3 < x < 0.42$ separates a phase with a TP coordination of alkali metal ($x < 0.3$) from a phase with a TAP coordination of alkali metal ($x > 0.42$). This second interpretation is consistent with a correlation proposed by Rouxel (*32*).

Application of the thermodynamic model to the measured sodium chemical potentials of Na_xTiS_2 is more complicated because of the reported chemical potential plateaus and structural observation of different phases (*8, 13, 20, 24*). Only the electrochemical data of Nagelberg and Worrell (*13*) has been used for reasons stated previously (*13*). Three distinct single-phase regions have been found by several authors (*8, 13, 24*) but values for their compositional ranges are in disagreement. Rouxel *et al.* (*24*) and Silbernagel and Whittingham (*8*) used crystallographic measurements to determine the phase boundaries, while Nagelberg and Worrell (*13*) extracted phase boundaries from their measured compositional variation of the sodium chemical potential. As with Na_xTaS_2, the contribution of the lattice expansion energy at concentrations above $x = 0.4$ is small. In the upper compositional range observed by Nagelberg and Worrell, $0.70 \lesssim x \lesssim 1.0$, the sodium chemical potential is conveniently expressed as a linear function of composition with a slope of 109 kJ/mole. Using the expression for the compositional variation of electron chemical potential given by Eq. (3), the pairwise interaction energy is found to be 10.9 ± 4 kJ/mole. A second single-phase region was observed for compositions $0.35 \lesssim x \lesssim 0.60$, with a linear compositional dependence and a pairwise interaction energy of 22.5 ± 4 kJ/mole. The third observed single-phase region observed by Nagelberg and Worrell was in the compositional range $0.10 \lesssim x < 0.23$, where the lattice expansion energy must be considered. For a compressibility of 30×10^{-13} cm²/dyne, the calculated pairwise interaction energy is 11.7 ± 6 kJ/mole using Eq. (5).

The best fit to the experimental data is shown by the three theoretical sodium chemical potential curves in Fig. 6 which

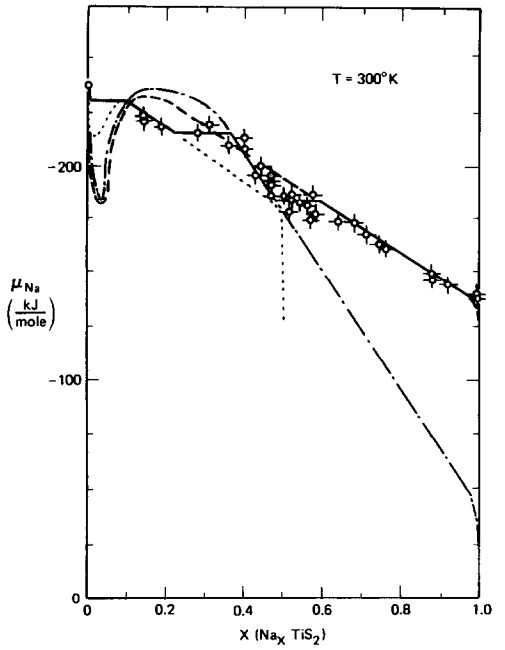

FIG. 6. Thermodynamic model curves for Na_xTiS_2 at 300 K (*13*): (---) assuming Stage I and TAP, ω = 11.7 kJ/mole and $k = 30 \times 10^{-13}$ cm²/dyne; (-·-) assuming Stage I and TP, ω = 22.6 kJ/mole and $k = 30 \times 10^{-13}$ cm²/dyne (· · · · ·) assuming Stage II and TAP, ω = 10.9 kJ/mole and $k = 30 \times 10^{-13}$ cm²/dyne.

are calculated by using the pairwise interaction energies given previously and compressibilities of 30×10^{-13} cm²/dyne and 20×10^{-13} cm²/dyne for TAP and TP sodium coordinations, respectively. A smaller compressibility for the trigonal prismatic coordination is reasonable since the sulfur atoms sit one on top of another. The two-phase chemical potential plateaus were determined by the equal areas criteria as given by Eq. (7). The chemical potential axis intercept of the linear portion of the curve is larger with sodium in a trigonal prismatic coordination ($0.35 \lesssim x \lesssim 0.60$) indicating a larger interaction between an inserted sodium atom and the TiS_2 layers. The limited compositional range of existence for the TP phase is due to the larger pairwise interaction energy and small compressibility. The interaction energies calculated for Na_xTiS_2 are summarized in Table I.

The similarity of the calculated repulsive interaction energies suggests that the sodium atoms in the low ($0.05 < x < 0.20$) and high ($0.70 < x < 1.0$) composition phases of Na_xTiS_2 reside in similar environments. Rouxel *et al.* (*24*) determined sodium coordination in their Stage I compounds ($0.38 < x < 0.67$ and $0.79 < x < 1.0$) to be trigonal prismatic and trigonal antiprismatic, respectively, but were unable to determine the sodium coordination in their Stage II compounds ($0.17 < x < 0.33$). In the ionicity diagrams proposed by Rouxel (*32*), the low composition phase lies in a stability phase region for a trigonal antiprismatic coordination, the same as the high-concentration phase. Nuclear magnetic resonance measurements also imply that the low- and high-concentration phases have similar coordinations for the sodium atom (*8*).

Application of the Model to the Lithium-Intercalated Disulfides

The compositional variations of lithium chemical potential for Li_xTiS_2 (*11*), Li_xTaS_2 (*12*), and Li_xVS_2 (*14*) have been measured. The results indicate a nearly linear increase of lithium chemical potential as the lithium content is increased. Application of the thermodynamic model yields the values for the lithium–lithium interaction energies given in Table I. The calculations assume the compositional variation of electron chemical potential shown in Fig. 1 and a compressibility of 30×10^{-13} cm²/dyne. The broken curves shown in Figs. 7 and 8 indicate that the lattice expansion energy contribution is negligible, presumably because of the smaller c-axis expansion of the lithium intercalated compounds (*3*). For example, in Fig. 7 for Li_xTaS_2, the calculated Stage II and Stage I lithium chemical potential curves almost coincide, with the

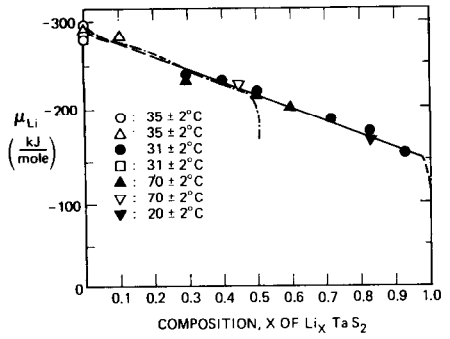

FIG. 7. Thermodynamic model curve for Li_xTaS_2 (*12*). Broken lines (– · –) represent curves generated by the model assuming Stage I; (– – –) assuming Stage II (for both, $k = 30 \times 10^{-13}$ cm²/dyne and $\omega = 17.2$ kJ/mole).

chemical potential difference being less than 0.5 kJ/mole. The small chemical potential difference implies that small extrinsic factors such as purity could easily cause a change from a Stage I compound to a Stage II compound.

The lithium chemical potential measured for Li_xTiS_2 by Whittingham (*11*) is nearly linear and can be easily fitted by the model with a lithium–lithium interaction energy of 2.9 kJ/mole as can be seen in Fig. 8. Thompson (*31*) has investigated in detail the lithium chemical potential composition relationships for Li_xTiS_2 by "Electrochemical Potential Spectroscopy." The compositional variation of $\Delta x/\Delta\mu_{Li}$ is found to exhibit several maxima which were associated with ordering of the intercalated lithium in the two-dimensional interlayer gap. The observed sharp maxima could also be explained by Eq. (*5*). The existence of very narrow two-phase fields would be predicted for the Stage II to Stage I transition.

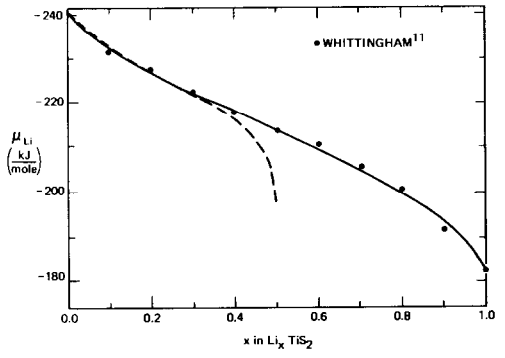

FIG. 8. Thermodynamic model curve for Li_xTiS_2 (*11*). Dashed line represents curve generated by model assuming Stage II compound with $k = 30 \times 10^{-13}$ cm²/dyne and $\omega = 2.9$ kJ/mole.

Application of the model to Li_xVS_2 (*14*) produces an interesting result. The observed variation of the lithium chemical potential ($\mu_{Li} \approx 245.11 - 38.6x$ kJ/mole) indicates a pairwise interaction energy of zero, when the variation of μ_F is given in Fig. 2. For the extreme case of no variation of the electron chemical potential with composition (μ_F = constant), the pairwise interaction energy would be ≈8.0 kJ/mole. In reality neither of the extreme cases ($\omega = 0$ or $d\mu_F/dx = 0$) probably exist.

Significance of the Calculated Repulsive Interaction Energies

The repulsive interaction between intercalated atoms can be estimated by the electrostatic repulsion of charged positive point charges, since the intercalated alkali metal atoms are almost completely ionized (*7–10*). Nearest neighbor intercalated atoms are separated by a distance equal to the a-axis lattice parameter (3–4 Å). At this distance the interaction energy between two positive charges would be, for example, 414 kJ/mole (4.3 eV) in TaS_2 intercalated compounds. This value is 12–20 times larger than the values tabulated in Table I. However, a reduction in the predicted interaction energy occurs when the disulfide electrons screen the positive ions from each other. The simple application of the Thomas–Fermi approximation (*33*) gives the screened interaction energy (E_I) as

$$E_I = 414\, e^{-\lambda r}(\text{kJ}), \qquad (8)$$

where $\lambda^2 \cong 4(n_0)^{1/2}/a_0$; r is the separation

distance assumed to be the a-axis lattice parameter, n_0 is the uniform electron density between charges, and a_0 is the Bohr radius. A list of the electron densities in TaS_2 needed to obtain various interaction energies is given in Table II. Reasonable values of the electron density ($\sim 10^{20}$ to $\sim 10^{21}$) are required in the interlayer gap to obtain the calculated values (17–35 kJ/mole) of the repulsive interaction energies for intercalated TaS_2 shown in Table I. Thus our calculated values are consistent with the assumption that the major factor establishing the interaction energies is a screened point charge.

An increased interaction energy is expected when a disulfide is intercalated with sodium instead of lithium, because sodium separates the disulfide layers significantly further than lithium and thus decreases the electron density between inserted atoms. A similar effect is expected when the intercalated atom coordination changes from the densely packed TAP coordination to the more separated TP coordination. The calculated values for ω tabulated in Table I are in accord with these two expectations.

TABLE II

CALCULATED COULOMBIC INTERACTION ENERGIES (E_I)

n_0 (electrons/cm^3)	Electrons/TaS_2 in $Na_{1.0}TaS_2$	E_I (kJ)
5.7×10^{23}	39.9	0.096
8.3×10^{22}	5.8	0.96
4.0×10^{22}	2.8	1.93
2.5×10^{22}	1.75	2.89
1.3×10^{22}	0.91	4.82
4.7×10^{21}	0.329	9.64
2.4×10^{21}	0.168	14.46
1.4×10^{21}	0.098	19.28
5.6×10^{20}	0.039	28.92
2.0×10^{20}	0.014	44.93

Conclusions

A thermodynamic model has been formulated to describe the observed compositional variation of alkali metal chemical potential in lithium and sodium intercalated disulfides. The important factors in determining the compositional variation of alkali metal chemical potential are the variation of electron chemical potential (μ_F), the interaction energy (ω) between intercalated atoms, the lattice expansion energy ($B(dc/dx)$) and the configurational entropy of filling vacant sites. In moderate compositional ranges the first two factors determined the observed chemical potential curves. However, the latter two factors determine the relative stability of Stage I and II compounds and therefore influence the location and size of two-phase regions. For example, the model predicts very similar lithium chemical potentials for both the Stage I and Stage II compounds when $x < 0.4$, since the lattice expansion enthalpy is very small.

Calculated values of the repulsive interaction energies (ω) tabulated in Table I were obtained using the compositional variation of electron chemical potential shown in Fig. 2. The repulsive interaction energy between intercalated atoms is greater for sodium atoms than for lithium atoms and is greater in tantalum disulfide than in titanium disulfide. Application of the thermodynamic model to Na_xTiS_2 indicates that repulsive interaction energies are greater for intercalated atoms in a trigonal prismatic (TP) coordination than in a trigonal antiprismatic (TAP) coordination.

Appendix: Derivation of Equilibria Criteria for Pseudo Binaries

When viewing a free-energy diagram, a pseudo-binary equilibrium between two phases occurs when the tangents to the free-energy curves lie on the same line. This condition is met when the chemical potentials of both constituents are equal in the two phases and the derivative of the

free-energy functions of the phases are equal. These two conditions are mathematically given by

$$\mu_{A1} = \mu_{A2} = \mu_A, \qquad \mu_{B1} = \mu_{B2} = \mu_B, \quad \text{(A1)}$$

$$\frac{dG_1}{dX_{A1}} = \frac{dG_2}{dX_{A2}}, \quad \text{(A2)}$$

where

G_i is the molar free energy of mixing for phase i, and

x_{Ai} is the mole fraction of A in phase i.

When the composition of the binary phases are represented as a interstitial compound, i.e., A_xB, the requirements given by Eqs. (A1) and (A2) can be rewritten. Nagelberg and Worrell (*13*) showed that for the compound A_xB,

$$G_{\text{mix}}(A_xB) = \int_0^x \mu_A\, dx, \quad \text{(A3)}$$

where G_{mix} is the free energy of mixing per A_xB.

Conversion to a free energy of mixing per gram-atom simply requires dividing by $(1 + x)$.

Equation (A2) can thus be rewritten using Eq. (A3) as

$$\frac{d\left\{\left[\int_0^{x''} \mu_{A1} dx\right] \Big/ (1 + x'')^2\right\}}{dx/(1 + x'')^2} = \frac{d\left\{\left[\int_0^{x'} \mu_{A2} dx\right] \Big/ (1 + x')^2\right\}}{dx/(1 + x')^2} \quad \text{(A4)}$$

where $x'' = x_{A1}$ and $x' = x_{A2}$. Rearranging and differentiating

$$(1 + x'')^2 \left[\frac{(1 + x'')\,\mu_{A1}\,dx - \int_0^{x''} \mu_{A1}\,dx}{(1 + x'')^2 dx}\right] = (1 + x')^2 \left[\frac{(1 + x')\,\mu_{A2}\,dx - \int_0^{x'} \mu_{A2}\,dx}{(1 + x')^2 dx}\right]. \quad \text{(A5)}$$

Simplifying

$$\mu_{A1} + x''\mu_{A1} - \int_{-\infty}^{x''} \mu_{A1}\,dx = \mu_{A2} + x'\,\mu_{A2} - \int_{-\infty}^{x'} \mu_{A2}\,dx. \quad \text{(A6)}$$

Using the equation for integration by parts and Eq. (A1),

$$\int_{-\infty}^{\mu_a} (x'' - x')\,d\mu_A = 0. \quad \text{(A7)}$$

The criteria for equilibrium given by Eq. (A7) is graphically shown in Fig. 5, in which the chemical potential increases from top to bottom to conform with cell-voltage–composition graphs. The equilibrium chemical potential is established by graphically determining the value which equates the area in the cross-hatched region of Fig. 5 to the lined area.

Acknowledgment

The authors would like to thank Dr. Geoffrey R. Belton for the initial suggestion of a two-dimensional chemisorption model. Financial support by the National Science Foundation–MRL Program, under Grant DMR 76-80994 is gratefully acknowledged.

References

1. B. C. H. STEELE, *in* "Critical Materials Problems in Energy Production" (C. Stein, Ed.), p. 711. Academic Press, New York (1976).
2. B. C. H. STEELE, *in* "Electrode Materials and Processes for Energy Conversion and Storage" (J. D. E. McIntyre, S. Srinivasan, and F. G. Will, Eds.), p. 799. Electrochemical Society, Princeton, N.J. (1977).
3. M. S. WHITTINGHAM, *Progr. Solid State Chem.* **12**, 41 (1978).
4. L. B. EBERT, *Annu. Rev. Mater. Sci.* **6**, 181 (1976).
5. *"Physics and Chemistry of Materials with Lay-*

ered Structures," Vol. 6, Reidel, Dordrecht (1976).
6. J. A. WILSON AND A. D. YOFFE, *Adv. in Phys.* **18,** 193 (1969).
7. A. LEBLANC-SOREAU, M. DANOT, L. TRICHET, AND J. ROUXEL, *Mater. Res. Bull.* **9,** 1960 (1974).
8. B. G. SILBERNAGEL, *Solid State Commun.* **17,** 301 (1975).
9. B. G. SILBERNAGEL AND M. S. WHITTINGHAM, *J. Chem. Phys.* **64,** 3670 (1976).
10. B. G. SILBERNAGEL AND M. S. WHITTINGHAM, *Mater. Res. Bull.* **11,** 29 (1976).
11. M. S. WHITTINGHAM, *J. Electrochem. Soc.* **123,** 315 (1976).
12. S. BASU AND W. L. WORRELL, *in* "Electrode Materials and Processes for Energy Conversion and Storage" (J. D. E. McIntyre, S. Srinivasan, and F. G. Will, Eds.), p. 861. Electrochemical Society, Princeton, N.J. (1977).
13. A. S. NAGELBERG AND W. L. WORRELL, *J. Solid State Chem.* **29,** 345 (1979).
14. D. W. MURPHY, J. M. CARIDES, F. S. DISALVO, C. CROS, AND J. V. WASZCZAK, *Mater. Res. Bull.* **12,** 825 (1977).
15. D. W. MURPHY, J. M. CARIDES, F. S. DISALVO, C. CROS, AND J. V. WASZCZAK, *Mater. Res. Bull.* **12,** 825 (1977).
16. D. A. WINN, J. M. SHEMILT, AND B. C. H. STEELE, *Mater. Res. Bull.* **11,** 559 (1976).
17. R. MCKINNON AND R. R. HAREING, *J. Solid State Ionics* **1,** 111 (1980).
18. M. ARMAND, Ph.D. Dissertation, Université Scientifique et Medicale et Institut National Polytechnique de Grenoble (1978).
19. A. H. THOMPSON, *J. Electrochem Soc.* **126,** 608 (1979).
20. I. LANGMUIR, *J. Amer. Chem. Soc.* **40,** 1361 (1918).
21. R. H. FOWLER AND E. A. GUGGENHEIM, "*Statistical Thermodynamics,*" p. 429. Cambridge Univ. Press, Cambridge (1960).
22. D. W. FISCHER, *Phys. Rev. B* **8**(8), 3576 (1973).
23. L. F. MATTHEISS, *Phys. Rev. B* **8**(8), 3719 (1973).
24. For example, J. A. ALONSO AND L. A. GIRAFALCO, *J. Phys. Chem. Solids* **39,** 79 (1978).
25. J. ROUXEL, M. DANOT, AND J. BICHON, *Bull. Soc. Chem. Fr.* **11,** 3930 (1971).
26. A. S. NAGELBERG, Ph.D. Dissertation, University of Pennsylvania (1978).
27. A. W. WEBB, J. L. FELDMAN, E. F. SKELTON, L. C. TOWLE, C. Y. LIV, AND I. L. SPAIN, *J. Phys. Chem. Solids* **37,** 329 (1976).
28. R. E. JONES, JR., H. R. SHANKS, D. K. FINNEMORE, AND B. MOROSIN, *Phys. Rev. B,* 835 (1972).
29. J. L. FELDMAN, *J. Phys. Chem. Solids* **37,** 1141 (1976).
30. H. D. FLACK, *J. Appl. Crystallogr.* **5,** 137 (1972).
31. E. WILHELM, *J. Chem. Phys.* **63,** 3379 (1975).
32. J. ROUXEL, *J. Solid State Chem.* **17,** 223 (1976).
33. C. KITTEL, "Introduction to Solid State Physics," 4th ed., p. 279. Wiley, New York (1971).